Mineralogia, vol. 54, 2023, 69-77 *Original Paper*

DOI: 10.2478/mipo-2023-0007

Thorite inclusions in zircon of the monzogranite, Lower Nubia, SW Egypt

Kamaleldin M. Hassan[1*], Irena Brunarska[2],

[1]Nuclear Materials Authority, El Katameya, New Cairo 3, Cairo Governorate 4710030, Egypt
[2]Institute of Geological Sciences, Jagiellonian University, Gronostajowa 3a, 30-387 Kraków, Poland

*Corresponding author: egy100@yahoo.com

Abstract

This report presents the results of a petrographical and mineralogical (optical microscopy, BSE-EDS image analysis) study of zircon in samples from the Lower Nubian monzogranite. The mineral occurs as smaller grains (< 80 µm) in a fine-grained quartz-feldspar-matrix, coexisting with other accessory minerals including biotite, clinochlore, titanite, and britholite-(Ce). Zircon is also present within biotite and britholite-(Ce), suggesting that it started crystallization at about the same time as these two minerals. Two types of thorite inclusions within zircon are reported in this study. Type 1 is widely distributed throughout the zircon grain, forming crystallites of which each is typically < 1 µm in size. Type 2 is relatively larger (5-15 µm) and occurs only in one part of the grain. For the thorite inclusions, three possible origins are briefly discussed: (1) exsolution of thorite from zircon; (2) dissolution/reprecipitation of zircon; and (3) growth syngenetically with zircon. Of these potential hypotheses, the syngenetic growth model seems more favorable for zircon-thorite intergrowths than the other two hypotheses. Thorite inclusions and their host zircons seem to have grown from magma rather than hydrothermal or supercritical solutions. Here, they have primary textures and consistent chemical compositions that are consistent with whole-rock geochemistry.

Keywords: Zircon, thorite, syngenetic inclusions, accessory minerals, metaluminous granite, Nubian Desert

1. Introduction

The lower Nubian monzogranite forms part of a larger body of granite rocks located in south-western Egypt (Fig. 1). Radiometrically, it is enriched in total field gamma (ɣ)-ray radiation (up to seven orders of magnitude more than the general radiation background) but without any obvious radioactive mineralization. The primary sources of ɣ-ray radiation are potassium (K), thorium (Th), and uranium (U), specifically the ^{40}K, ^{232}Th, and ^{238}U decay chains (Hassan 2007). Concentrations of K = 44000, Th = 51, U = 10, and rare earth elements (REE) = 297 ppm, respectively (Hassan 2023). Most of K is resided in feldspars and micas, while the U, Th, and REE are incorporated into accessory minerals. While some accessory minerals such as biotite, clinochlore, titanite, and britholite-(Ce) have been considered previously (Hassan 2008, 2023), others such as zircon have rarely been investigated. Here, the authors present the first results derived from optical microscopy, backscattered-electron (BSE) imaging, and energy dispersive X-ray spectroscopy (EDS) performed on zircon grains in samples of the Lower Nubian monzogranite. The main objective is to characterize thorite inclusions in the grains and to determine their petrogenesis. The results of this study enhance our knowledge of the zircon-thorite mineral group in metaluminous granites, as well as contribute to the petrography of the host rock—a fertile source for thorium in south-western Egypt.

2. Geological Background

The Lower Nubia (Fig. 1) is a hyperarid desert, with very hot summers and very little, if any, rainfall. Much of the desert is a land where some of the sandstone overlay has been eroded away and the underlying "basement complex" of granite rocks is exposed at the surface, resulting in topography of rugged ridges. The granites are related to the tonalite magma emplaced in successive phases containing biotite, hornblende or both during the Proterozoic in south-western Egypt (Sabet 1972; List et al. 1989).They comprise of four different types of rocks: (1) monzogranite, (2) granodiorite, (3) tonalite, and (4) monzonite (Hassan 2008). These rocks occur in the form of small residual boulders often buried partially or completely by Nubian sand. The boulders are the remnants of a mountain subjected to erosion weathering which is evident from the abundance of granite debris and soil material in the area. The soil does not have a developed profile and is largely medium to coarse-grained. Mineralogically, it comprises quartz, albite, illite, hematite, and biotite (Hassan, Gunnlaugsson 2013).

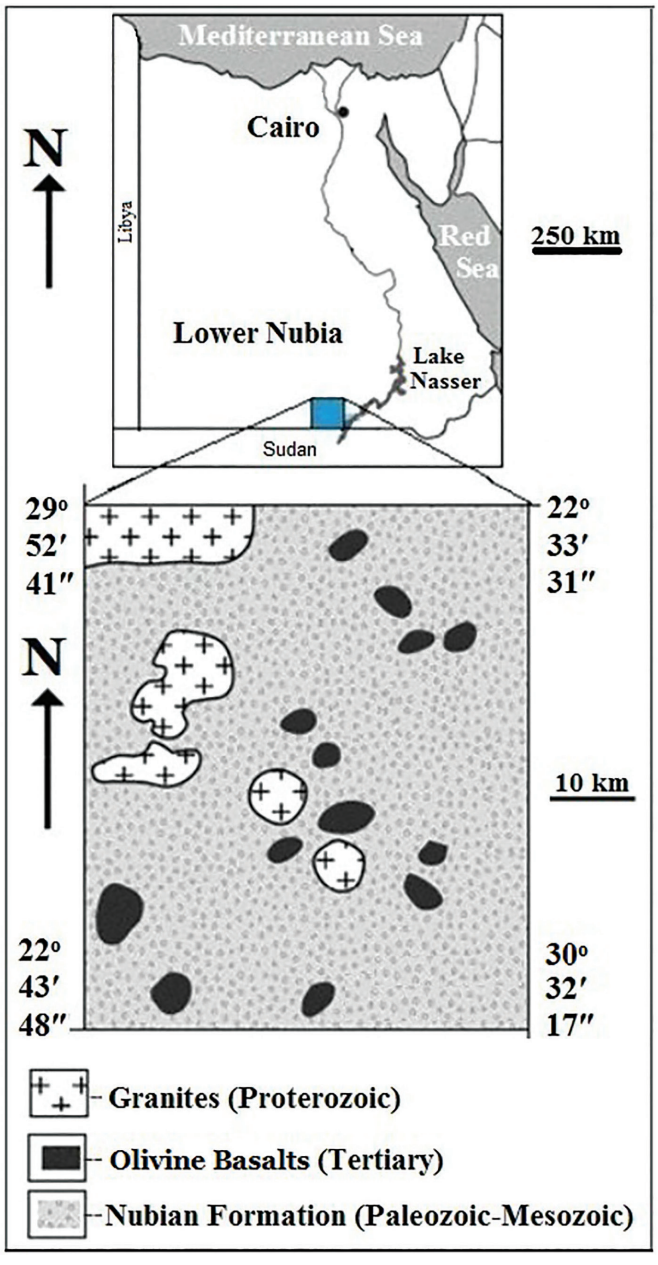

Figure 1. Geological map of south-western Egypt (Revised from GSMA 1981).

3. Methods

Samples of the Lower Nubian monzogranite, previously studied (Hassan 2023) are used for this research. Chemically, they are metaluminous (A/CNK ~ 0.9), have a high acidic signature (SiO_2 ~ 71 wt%) and a moderate europium anomaly (Eu/Eu* = 0.71). *M*icroscopic examinations of the samples were performed on thin polished sections using conventional optical methods in transmitted and reflected light (a polarizing microscope Olympus BX41) at the Nuclear Materials Authority, El Katameya, Egypt. In addition, selected minerals in carbon-coated thin sections were analyzed with a field-emission scanning electron microscope (FE-SEM, Hitachi S-4700) attached to a Norman Vantage EDS at the Institute of Geological Sciences of the Jagiellonian University, Kraków, Poland. FE-SEM operation conditions are: (1) accelerating voltage = 20 kV, (2) working distance = 12 mm, (3) emission current = 10 nA, (4) beam diameter < 1 um, and (5) counting time (live time limit) = 100 seconds. For each analyzed area within the selected mineral, several points were randomly measured to ensure its homogeneity. The correction procedure (Phi-Rho-Z) was employed for raw data before normalizing the EDX data. Duplicate samples were analyzed and the results were within the accepted values.

4. Results

In hand specimens, the Lower Nubian monzogranite is seen to exhibit a slightly gneissose texture in which light minerals form much thicker layers than the mafic minerals that constitute thin streaks. The light minerals are plagioclase, potash feldspar, and quartz, while the mafic ones are biotite partially altered to clinochlore (Fig. 2A). Plagioclase (mainly oligoclase) occurs as subidiomorphic to xenomorphic crystals partially altered to sericite and epidote. The potash feldspar is represented by orthoclase and microcline, exhibiting perthitic texture and partially transformed to clay. Quartz occurs as strained flattened crystals due to mylonitization. Small crystals of quartz are sometimes enclosed in plagioclases, while the coarse ones always show undulose extinction. The accessory minerals found in the examined samples are: zircon > titanite > britholite-(Ce) (Figs. 2A, B). Zircon grains are remarkably abundant throughout the sample, but they are small, typically between 20 and 80 µm. Titanite forms diamond-shaped crystals of very high relief and has a brown or red-brown color. Britholite-(Ce) typically has a platy habit and forms crystals ranging in size from ~ 200 to 600 µm.

Small zircon grains are present within britholite-(Ce) (Fig. 2B) and biotite (Fig. 2C). The included zircon in biotite exhibits a cloudy appearance where the cracks are formed. This zircon is also surrounded by brown

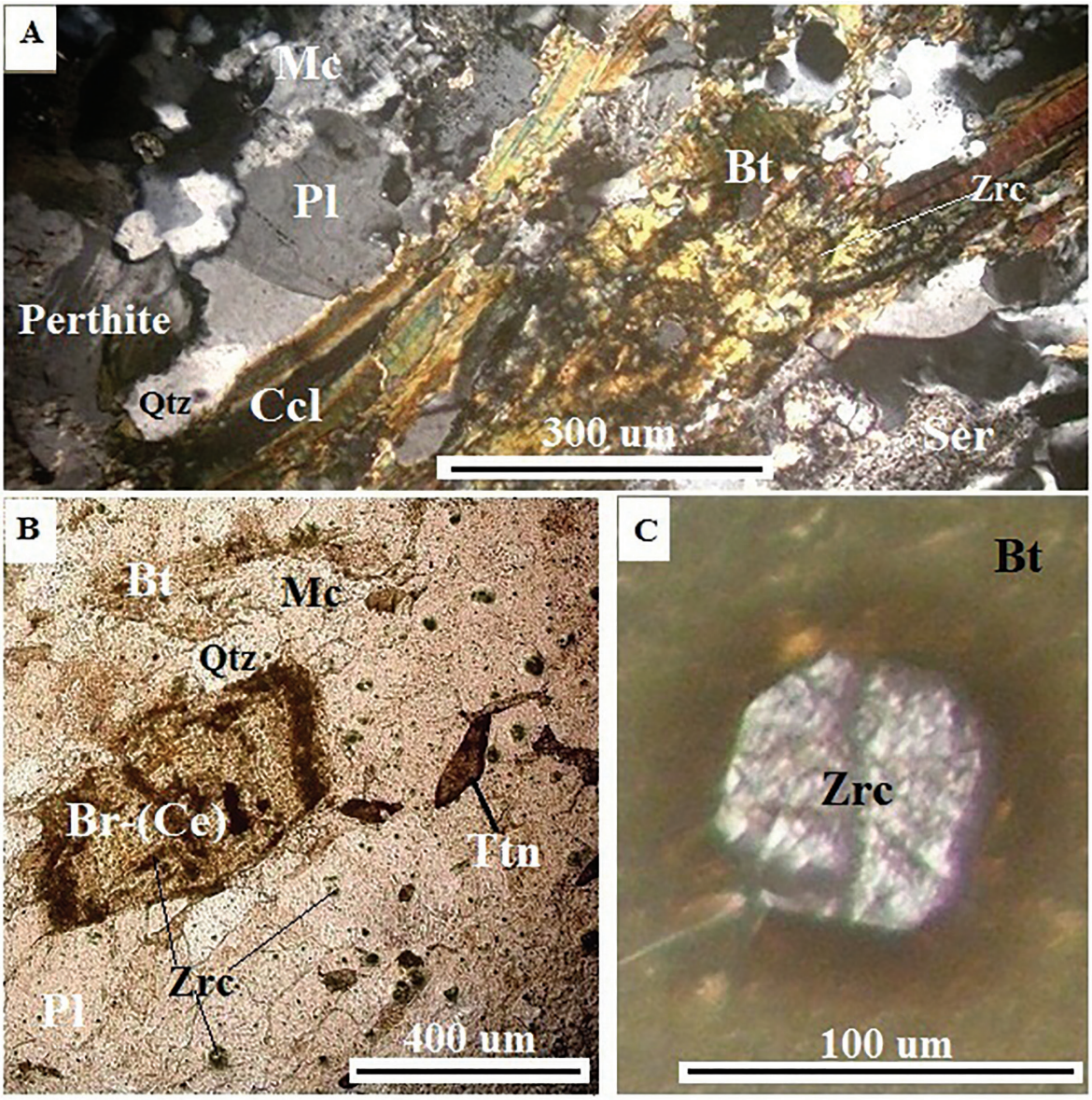

Figure 2. Optical microscope images of the Lower Nubian monzogranite. (A) Image in cross-polarized light showing a gneissose texture—the segregation of felsic (feldspars and quartz) and mafic minerals (biotite and its alteration product clinochlore). (B) Image in plane-polarized light showing numerous grains of zircon widely distributed throughout the thin section. (C) Image in cross-polarized light for radioactive halos or pleochroic halos (burnt mark) around zircon enclosed in biotite and having a cloudy altered appearance. Mineral abbreviations in alphabetical order: Bt—biotite, Br-(Ce)—britholite-cerium, Ccl—clinochlore, Mc—microcline, Pl— plagioclase, Qtz—quartz, Ser—sercite, Ttn—titanite, Zrc—zircon.

halos—the products of high energy α-particle emitted from radionuclides incorporated into the zircon structure.

Typical petrographic features of zircon grains in the samples of the Lower Nubian monzogranite are shown in the BSE images (Figs. 3-5). Most grains are euhedral or have a slight to moderate rounding of crystal edges and terminations. Elbow twins are also seen (Fig. 3A). Some grains display some embayment and therefore corrosion (Figs. 3A, 4A and 5B). The others are often fractured (most likely due to extremely poorly polished thin sections), but they appear preserved as expected for zircon in igneous rocks.

Two kinds of thorite inclusions within zircon are revealed in BSE images. These are: (1) smaller thorite inclusions (Fig. 4) and larger thorite inclusions (Fig. 5). The former occur in the forms of randomly scattered, bright-colored crystallites of which each varies in size from ~ one-tenth of micrometer up to ~ 2 µm. The larger thorite inclusions (5-15 µm), on the other hand, are present only in one part of the host zircon.

Representative EDS analyses of the smaller and larger thorite inclusions as well as their host zircons are given in Table 1, and so are the formulae of zircon and thorite calculated based on 4 oxygens. The results of different samples are comparable with analytical data from other occurrences (Pointer et al. 1988; Žáček et al. 2009). Only the EDS analyses of smaller thorite inclusions are far outside the range expected for thorite composition. This is due to the fact that any EDS analysis on small thorite inclusions surely acquires signals from both the host zircon and the inclusion itself. The spatial resolutions of EDS measurements cannot be < 1 or 2 microns, the

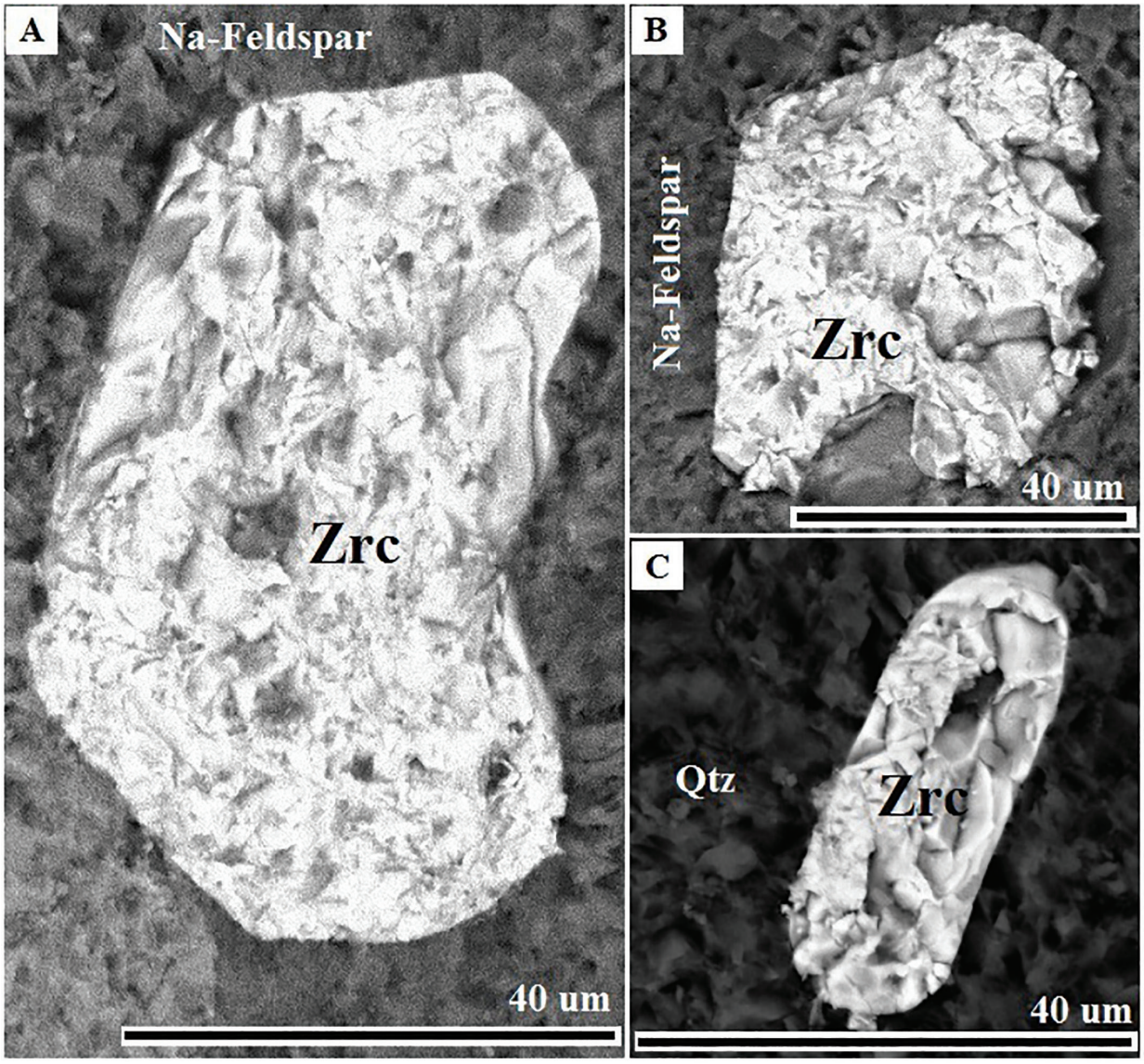

Figure 3. BSE images of zircon grains in the studied samples: (A) Elbow-shaped zircon twin showing corrosion embayment on the right side of the grain. (B) Stubby zircon prism with one pyramidal termination and having vertical fractures and broken parts. (C) Corroded zircon prism, with weakly-rounded edges.

exact size of the smaller thorite inclusions is shown in Fig. 4.

5. Discussion

In the Lower Nubian monzogranite, zircon forms in a fine-grained, feldspar-quartz matrix, coexisting with other accessory minerals including biotite, titanite, and britholite-(Ce). It is also included in biotite and britholite-(Ce), leading to the conclusion that zircon started crystallization at approximately the same time as the other two minerals. The formation of elbow twinning in zircons (Fig. 3A) indicates a sudden variation in the rate of crystallization (e.g. Jocelyn, Pidgeon 1974; Kabesh et al. 1976; Corfu et al. 2003). Rounded zircons (Figs. 4B and 5B) are likely produced during cooling of the magma in which the mineral crystallized (Spotts 1962; Hassan 1985; Higazy et al. 1986).

Zircon in the Lower Nubian monzogranite shows different features. The primary magmatic zircon with a narrow range of chemical variability approaches the stoichiometric composition, with Σ cations = 2.01-2.09 apfu (Table 1). The content of ThO_2 and REE_2O_3 is below detection limit in all 7 zircon analyses while the UO_2 and Hf_2O_3 are detected in 3 of these analyses (Table 1). Contents of UO_2 and Hf_2O_3 are from 0.29 to 0.89 and from 1.15 to 1.57 wt%, respectively. Studies indicate that magmatic zircon contains up to 0.5 wt% ThO_2 and 2 wt% UO_2 (Heaman, Parrish 1991). Other work has shown hafnium to be present in all naturally-occurring zircon, mostly in the range 0.5-1.5 wt% Hf_2O_3 (Wang et al. 2010). Zircon grains in this study show relatively high values of K_2O, Na_2O, CaO, Fe_2O_3, and Al_2O_3. These chemical patterns partly agree with the conclusion of Geisler et al. (2003) who indicated, based on hydrothermal experimental work, that altered parts of zircon gained solvent cations (e.g. Ca^{2+}, Mg^{2+}, Al^{3+}) and lost variable quantities of Zr, Si, Hf, REE, U as well as radiogenic Pb.

The zircon of the Lower Nubian monzogranite contains two morphologically distinct types of thorite inclusions: (1) small thorite inclusions occurring in different parts

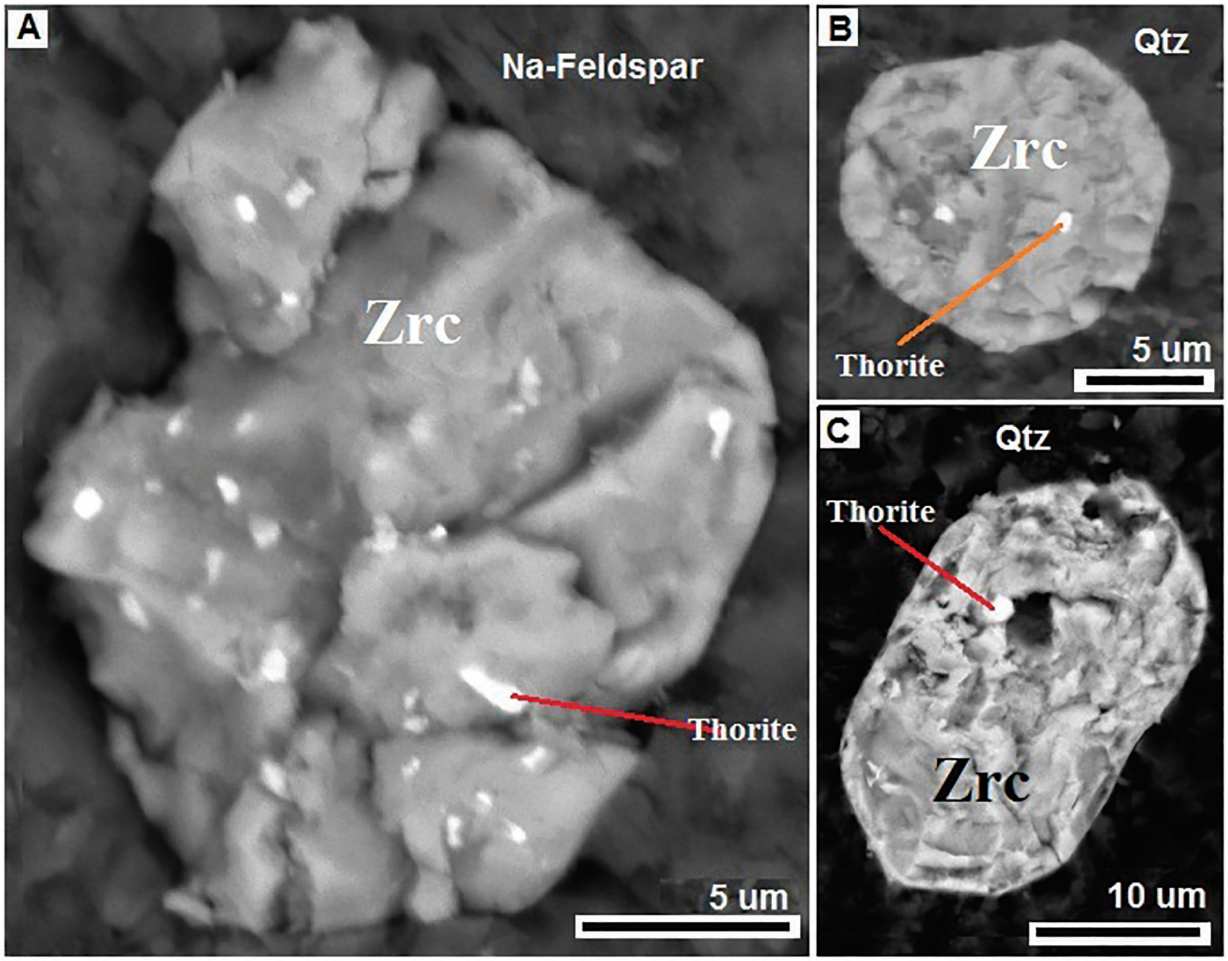

Figure 4. BSE images of zircon grains in the studied samples showing small micro-inclusions of thorite (white areas). (A) Pentagonal cone-shaped grain showing corrosion embayment on the upper left side of the grain. (B) Grain with slightly rounded edges. (C) Euhedral grain with unequally developed bipyramids, showing grooves and eroded surfaces.

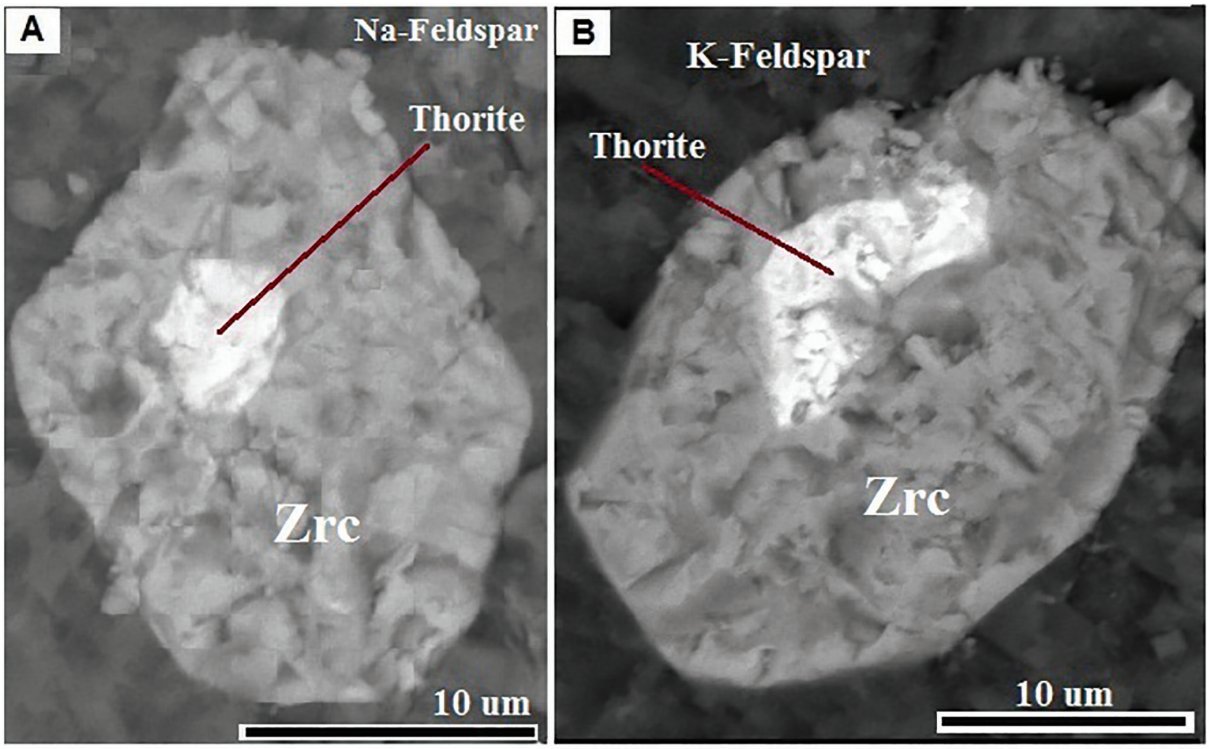

Figure 5. BSE images of zircon grains in the studied samples containing larger micro-inclusions of thorite (white areas). (A) Heptagonal shape grain. (B) Another heptagonal grain slightly rounded edges, and corrosion embayment on the upper side of the grain.

Table 1. Representative SEM-EDS analyses (wt %, above) and corresponding structural formulae [4 (O) apfu, below] for zircon and its thorite inclusions from the Nubian monzogranite.

	Primary magmatic zircon							Smaller thorite inclusions				Larger thorite inclusions				
	1	2	3	4	5	6	7	8	9	10	11	12	13	14	15	16
SiO_2	29.06	29.47	29.53	29.81	30.42	29.85	31.59	29.77	28.52	31.17	30.24	24.71	26.08	19.12	25.32	22.81
ThO_2	BDL	BDL	BDL	BDL	BDL	BDL	BDL	3.12	6.61	3.71	11.56	47.97	65.98	53.18	67.02	48.69
UO_2	BDL	0.45	0.29	BDL	BDL	BDL	0.89	BDL	BDL	BDL	BDL	14.08	BDL	15.15	BDL	11.85
Al_2O_3	0.46	BDL	BDL	BDL	BDL	0.64	BDL	0.21	BDL	1.55	1.89	1.82	1.30	0.72	1.33	1.29
Ce_2O_3	BDL	BDL	BDL	BDL	BDL	BDL	BDL	BDL	BDL	BDL	BDL	1.70	BDL	BDL	BDL	1.91
Nd_2O_3	BDL	BDL	BDL	BDL	BDL	BDL	BDL	BDL	BDL	BDL	BDL	1.57	BDL	BDL	BDL	1.61
Fe_2O_3	0.75	BDL	0.27	BDL	0.28	0.33	0.64	BDL	0.63	0.89	1.07	BDL	BDL	BDL	BDL	BDL
ZrO_2	67.31	69.48	69.19	68.12	69.92	66.35	65.66	65.15	63.29	59.58	50.13	5.66	5.70	9.66	1.94	10.04
HfO_2	1.57	BDL	BDL	1.15	BDL	1.17	BDL	BDL	BDL	BDL	1.44	BDL	BDL	BDL	BDL	BDL
MgO	0.15	BDL	BDL	BDL	BDL	BDL	0.21	BDL	BDL	0.16	BDL	BDL	BDL	BDL	BDL	BDL
CaO	BDL	BDL	BDL	0.40	BDL	0.73	0.27	0.92	0.57	1.19	1.38	1.59	BDL	1.38	3.05	1.19
Na_2O	0.41	0.29	0.46	BDL	0.39	0.59	0.50	0.83	0.38	0.72	1.21	0.90	0.94	0.80	1.33	0.61
K_2O	0.26	0.30	0.25	0.52	BDL	0.34	0.24	BDL	BDL	1.02	1.08	BDL	BDL	BDL	BDL	BDL
Total	99.97	99.99	99.99	100.00	101.1	100.00	100.00	100.00	100.00	99.99	100.00	100.00	100.00	100.01	99.99	100.00
Si	0.93	0.92	0.90	0.94	0.94	0.93	0.97	0.94	0.92	0.97	0.99	1.10	1.15	0.94	1.13	1.07
Th	-	-	-	-	-	-	-	0.02	0.05	0.02	0.08	0.48	0.66	0.59	0.68	0.52
U	-	0.00	0.00	-	-	-	0.01	-	-	-	-	0.13	-	0.16	-	0.13
Al	0.04	-	-	-	-	0.05	-	0.02	-	0.13	0.16	0.09	0.15	0.09	0.07	0.16
Ce	-	-	-	-	-	-	-	-	-	-	-	0.03	-	-	-	0.07
Nd	-	-	-	-	-	-	-	-	-	-	-	0.02	-	-	-	0.06
Fe	0.01	-	0.01	-	0.01	0.02	0.03	-	0.06	0.07	0.06	-	-	-	-	-
Zr	1.04	1.06	1.06	1.04	1.05	1.01	0.99	1.01	1.00	0.90	0.79	0.12	0.12	0.23	0.04	0.22
Hf	0.01	-	-	0.01	-	0.01	-	-	-	-	0.01	-	-	-	-	-
Mg	0.01	-	-	-	-	-	0.01	-	-	0.00	-	-	-	-	-	-
Ca	-	-	-	0.01	-	0.02	0.01	0.03	0.02	0.02	0.04	0.08	-	0.07	0.13	0.06
Na	0.03	0.02	0.03	-	0.02	0.04	0.03	0.04	0.02	0.04	0.08	0.05	0.08	0.05	0.11	0.05
K	0.01	0.01	0.01	0.02	-	0.01	0.01	-	-	0.01	0.04	-	-	-	-	-
Sum	2.08	2.01	2.01	2.02	2.02	2.09	2.06	2.06	2.07	2.16	2.25	2.10	2.16	2.13	2.16	2.34

BDL, below detection limit.

of zircon grains as bright-colored crystallites (Fig. 4) and (2) larger thorite inclusions occurring only in one part of the zircon (Fig. 5). For the larger and smaller thorite inclusions, three possible origins might be proposed: (1) exsolution of thorite from zircon; (2) dissolution/reprecipitation of zircon; and (3) growth syngenetically with zircon. Exsolution is a solid-state recrystallisation process. Zircon forms solid solutions with the other members of zircon-group minerals including, but they are not limited to, Hafnon ($HfSiO_4$), thorite ($ThSiO_4$), coffinite ($USiO_4$), and xenotime (YPO_4) (Finich, Hancher 2003). Of these minerals, Hafnon forms a complete solid solution with zircon (Correia Neves et al. 1974). However, the substitution of thorite in the zircon structure is limited even at higher temperatures (~ 4 mol%; Mumpton, Roy 1961). The solid solution tends to exsolve the thorite in order to reduce strain energy created by the substitution of theTh^{4+} cation (0.94 Å) for the smaller Zr^{4+} (0.72 Å). The occurrence of thorite inclusions in metasomatised zircon from Nigeria is attributed to exsolution following metastable growth of Th, U-rich zircon (Pointer et al. (1998). Such mechanism is considered unlikely in zircon of the Lower Nubian monzogranite because it is depleted in thorium and uranium.

Zircon with high U or Th contents often becomes metamict (amorphous) and more susceptible to fluid influence. Zircon with high contents of light rare-earth elements (LREE), Na, Ta and other incompatible elements is also more soluble (Xia et al. 2010). Under fluid influence, these zircons can be replaced by new zircon material with higher crystallinity. The new zircon phase occupies a smaller volume compared to the dissolving amorphous phase and the volume deficit is compensated by pores (Kaulina et al. 2010). Therefore, zircon formed by dissolution-reprecipitation has a spongy texture (Hoskin et al. 1998; Schmitt 2006; Xie et al. 2005) in addition to the presence of "exsolved" accessory phases like thorite, thorianite, and xenotime (Schmitt 2006). Such zircon is similar to that of hydrothermal origin, which appears as "veinlets or filaments" in host rock, contains many thorite inclusions, and has abundances of LREE, Na, Ta and other incompatible elements (Rubin et al. 1989). The typical characteristics of zircon of dissolution-reprecipitation and hydrothermal origins are absent in the zircon of the investigated Lower Nubian monzogranite. Thus, the monzogranite zircons would have grown from magma, rather than secondary solutions.

The Lower Nubian monzogranite zircon has ~ 7 times more thorium than the Earth's crust (Mason 1966). Whole-rock Th/U ratios are ~ 5.0 (Hassan 2023) as seen in magmatic rocks (Wedepohl 1995; Hassan 2018), while rocks influenced by hydrothermal fluids have higher values (Wedepohl 1995). The morphology of thorite inclusions and their host zircons strongly suggest that they are "syngenetic", formed simultaneously and from the same chemical processes. The coexistence of thorite-containing and thorite-free parts in single zircon grains can be explained as follows. Thorite crystals formed in the melt a little earlier, and then zircon grew around them. In some places there were more thorite crystals; in others there were very fewer. This is where the pure zircons were formed. Thorite inclusions (Figs. 4 and 5) appear unbroken and show no evidence of surface etching or corrosion. These inclusions, like their host zircon, are depleted in REE and other rare metals. The morphology and distributions of thorite inclusions into zircon grains are similar to those reported from other studies (Alekseev et al. 2014; Sorokhtina el. 2016; Spiridonov et al. 2018) where they are interpreted as syngenetic inclusions.

6. Conclusions

In the Lower Nubian monzogranite, zircons are numerous, but small (20-80 µm). They occur in feldspars and quartz as well as are included within the biotite and britholite-(Ce). The petrographic relations suggest a wide range of zircon crystallization during the solidification of the parent magma. Some zircon grains contain inclusions of thorite, ranging in size from ~ 0.1 to ~ 15 µm. Three models were taken into account for origins of zircon-thorite intergrowths: exsolution of thorite from zircon; dissolution/reprecipitation of zircon; and syngenetic crystallization. The syngenetic crystallization model seems more favorable for zircon-thorite intergrowths than the other two models. The intergrowths would have resulted from magmatic solutions, rather than hydrothermal or supercritical fluids. Here, the zircon and its thorite inclusions have primary textures and consistent compositions. These characteristics are also consistent with whole-rock geochemistry.

Competing Interests

The authors declare no competing interests.

Acknowledgments

The first author acknowledges the staff of the "Toshka Uranium Study and Evaluation Project", the Egyptian Nuclear Materials Authority (ENMA) for field assistance. Thanks are to E. K. Abu Zeid of the ENMA for access to his petrography laboratory. Special thanks to the Associate Editor S. Ferrero and an anonymous reviewer who helped our manuscript reach level of clarity for publication.

References

Alekseev, V. I., Polyakova, E. V., Machevariani, M. M., & Marin, Yu. B. (2014). Evolution of zircons from postorogenic intrusive series with Li–F granites, Russian Far East. *Geology of Ore Deposits*, *56*, 513–530. https://doi.org/10.1134/S1075701514070034.

Corfu, F., Hanchar, J. M., Hoskin, P. W. O., & Kinny, P. (2003). Atlas of zircon textures. *Reviews in Mineralogy and Geochemistry*, *53*, 469–500. DOI: 10.2113/0530469.

Correia Neves, J. M., Lopes Nunes, J. E., & Sahama, T. G. (1974). High hafnian members of the zircon-hafnon series from

the granite pegmatites of Zambézia, Mozambique. *Contributions to Mineralogy and Petrology*, *48*, 73–80. DOI: 10.1007/BF00399111.

Finch, R. J., Hanchar, J. M. (2003). Structure and Chemistry of zircon and zircon-group minerals. *Reviews in Mineralogy and Geochemistry*, *53*, 1–25. DOI: 10.2113/0530001.

Geisler, T., Pidgeon, R. T., Kurtz, R., van Bronswijk, W., & Schleicher, H. (2003). Experimental hydrothermal alteration of partially metamict zircon. *American Mineralogist*, *88*, 1496–1543. DOI: 10.2138/am-2003-1013.

GSMA. (1981). Geological map of Egypt, scale 1:2,000,000. Geological Survey and Mining Authority, Abbasyia, Cairo, Egypt.

Hassan, K. M. (1985). A study of the heavy minerals of some granitic plutons in the northern part of the Eastern Desert, Egypt as a guide to their petrogenesis. MS. Thesis. Azhar University, Cairo, Egypt.

Hassan, K. M. (2007). Review ionizing radiation in the environments. *Isotope and Radiation Research*, *39*, 743–662. https://inis.iaea.org/search/search.aspx?orig_q=RN:39022119.

Hassan, K. M. (2008). Petrography, chemistry and radioactivity of granitoids at north Gebel Seri, South Western Desert, Egypt. *Isotope and Radiation Research, 40*, 615–629. https://inis.iaea.org/search/search.aspx?orig_q=RN:40047318.

Hassan, K. M. (2018). Trace elements and REE enrichment at Seboah Hill, SW Egypt. *Mineralogia*, *49*, 47–65. DOI: 10.2478/mipo-2018-0007.

Hassan, K. M. (2023). Britholite-(Ce) from the metaluminous granite of SW Egypt. *Mineralogia*, *54*, 11–17. DOI: 10.2478/mipo-2023-0002.

Hassan, K. M., & Gunnlaugsson, H. P. (2013). Characterization of barren, granitic soils from the Nubian Desert (SW Egypt) by ^{57}Fe Mössbauer spectroscopy. *Mineralogia*, *44*, 39-51. DOI: 10.2478/mipo-2013-0004.

Heaman, L., & Parrish, R. (1991). U-Pb geochronology of accessory minerals. In Short course handbook on applications of radiogenic isotope systems to problems in geology (Heaman, L., & Ludden, J. N. eds.). Mineralogical Association of Canada (59–102).

Higazy, M., Abu El-Leil, I., & Mokhtar, K. (1986). Statistical study of zircon as a guide to the origin and type of granitic rocks, Northern Eastern Desert, Egypt. *Annals of the Geological Survey of Egypt*, *16*, 309–314.

Hoskin, P. W. O., Kinny, P. D., & Wyborn, D. (1998). Chemistry of hydrothermal zircon: investigating timing and nature of water-rock interaction. In Water-Rock Interaction, WRI-9 (Arehart,G. B., & Hulston, J. R. eds.). AA Balkema, Rotterdam (545–548).

Jocelyn, J., & Pidgeon, R. T. (1974). Examples of twinning and parallel growth in zircons from some Precambrian granites and gneisses. *Mineralogical Magazine*, *39*, 587–594.

Kabesh, M. L., Refaat, A. M., & Abdallah, Z. M. (1976). The significance of zircon as a guide to the petrogenesis of granites from Ras Barud area, Eastern Desert, Egypt. *Kuwait Journal of Science*, *3*, 207–216.

Kaulina, T., Lyalina, L., Kamenetsky, V., Il'Chenko, V., Bocharov, V., & Gannibal, M. (2020). Composition and Structure of Zircon from Hydrothermal Uranium Occurrences of the Litsa Ore Area (Kola Region, Russia). *Geosciences 10*, 278. DOI: 10.3390/geosciences10080278.

List, F. K., El-Gaby, S., & Tehrani, R. (1989). The basement rocks in the Eastern and Western Deserts and Sinai. In Stratigraphic lexicon and explanatory note to the geologic map of Egypt 1:500000 (Hermina, M., Klitzsch, E. & List, F. eds.). Egyptian General Petroleum Corporation, Cairo, Egypt (33–56).

Mason, B. (1966). Principle of Geochemistry. Third edition. John Willey and Sons Inc., New York.

Mumpton, F. A., & Roy, R. (1961). Hydrothermal stability studies of the zircon-thorite group. *Geochimica et Cosmochimica Acta*, *21*, 217–238. https://doi.org/10.1016/S0016-7037(61)80056-2.

Pointer, C. M., Ashworth, J. R., & Ixer, R. A. (1988). The zircon–thorite mineral group in metasomatized granite, Ririwai, Nigeria 2. Zoning, alteration and exsolution in zircon. *Mineralogy and Petrology*, *39*, 21–37. https://doi.org/10.1007/BF01226260.

Rubin, J. N., Henry, C. D., & Price, G. (1989). Hydrothermal zircons and zircon overgrowths, Sierra Blanca Peaks, Texas. *American Mineralogist*, *74*, 865–869. http://www.minsocam.org/ammin/AM74/AM74_865.pdf.

Sabet, A. H. (1972). On the stratigraphy of basement rocks of Egypt. *Annals of the Geological Survey of Egypt*, *II*, 79–102.

Schmitt, A. K. (2006). Laacher See revisited: high-spatial-resolution zircon dating indicates rapid formation of a zoned magma chamber. *Geology*, *34*, 597–600. https://doi.org/10.1130/G22533.1.

Sorokhtina, N. V., Kogarko, L. N., Shpachenko, A. K., & Senin, V. G. (2016). Composition and conditions of crystallization of zircon from the rare-metal ores of the Gremyakha–Vyrmes Massif, Kola Peninsula. *Geochemistry International*, *54*, 1035–1048. https://doi.org/10.1134/S0016702916120119.

Spiridonov, E. M., Filimonov, S. V., Semikolennykh, E. S., Korotaevaa, N. N., & Krivitskaya, N. N. (2018). Zirconolite, baddeleyite, zircon, and thorite of island-arc quartz gabbronorite-dolerites of the Ayu-Dag Intrusive, Crimean Mountains. *Moscow University Geology Bulletin*, *73*, 538–548. DOI: 10.3103/S0145875218060121.

Spotts, J. H. (1962). Zircon and other accessory minerals. Coast Range batholith, California. *Geological Society of America Bulletin*, *73*, 1221–1240. https://doi.org/10.1130/0016-7606(1962)73[1221:ZAOAMC]2.0.CO;2.

Wang, X., Griffin, W., & Chen, J. (2010). Hf contents and Zr/Hf ratios in granitic zircons. *Geochemical Journal*, *44*, 65–72. https://doi.org/10.2343/geochemj.1.0043.

Wedepohl, K. H. (1995). The composition of the continental crust. *Geochimica et Cosmochimica Acta*, *59*, 1217–1232. http://dx.doi.org/10.1016/0016-7037(95)00038-2.

Xie, L., Wang, R., Chen, X., Qui, J., & Wang, D. (2005). Th-rich zircon from peralkaline A-type granite: mineralogical features and petrological implications. *Chinese Science Bulletin*, *50*, 809–817. https://doi.org/10.1007/BF03183683.

Xia, Q. X., Zheng, Y. F., & Hu, Z. C. (2010). Trace elements in zircon and coexisting minerals from low-T/UHP

metagranite in the Dabie orogen: implications for action of supercritical fluid during continental subduction-zone metamorphism. *Lithos*, *114*, 385–412. https://doi.org/10.1016/j.lithos.2009.09.013.

Žáček, V., Škoda, R., & Sulovsky, P. (2009). U–Th-rich zircon, thorite and allanite-(Ce) as main carriers of radioactivity in the highly radioactive ultrapotassic melasyenite porphyry from the Šumava Mts., Moldanubian Zone. *Czech Republic Journal of Geosciences*, *54*, 343–354. DOI: 10.3190/jgeosci.053.

Received: 15 Sep 2023
Accepted: 22 Nov 2023
Handling Editor: Silvio Ferrero